



Hot mantle upwelling across the 660 beneath Yellowstone

Brandon Schmandt ^{a,*}, Kenneth Dueker ^b, Eugene Humphreys ^c, Steven Hansen ^b

^a Seismological Laboratory, California Institute of Technology, Pasadena, CA 91125, USA

^b Department of Geology and Geophysics, University of Wyoming, Laramie, WY 82071, USA

^c Department of Geological Sciences, University of Oregon, Eugene, OR 97403, USA

ARTICLE INFO

Article history:

Received 31 December 2011

Received in revised form 13 March 2012

Accepted 15 March 2012

Available online 13 April 2012

Editor: P. Shearer

Keywords:

Yellowstone hotspot

mantle transition zone

mantle convection

mantle plumes

ABSTRACT

P-to-s receiver functions mapped to depth through P and S body-wave tomography models image continuous 410 and 660 km discontinuities beneath the area covered by USArray prior to the year 2011. Mean depths to the 410 and 660 km discontinuities of 410 and 656 km imply a mantle transition zone that is about 4 km thicker than the global average and hence has a slightly cooler mean temperature and/or enhanced water content. Compared to the mean 660 depth beneath this ~2000 km wide area, the 660 beneath the Yellowstone hotspot is deflected upward by 12–18 km over an area about 200 km wide. This is the most anomalous shallowing of the 660 imaged and its horizontal extent is similar to the area where P and S tomography image low-velocity mantle extending from the top of the transition zone to about 900 km depth. Together, these results indicate a high-temperature, plume-like upwelling extending across the 660. The depth of 410 km discontinuity beneath the Yellowstone region is within 5 km of the mean depth implying that the plume is vertically heterogeneous and possibly discontinuous. Tomography indicates a similar vertically heterogeneous thermal plume. The irregular plume structure may be intrinsic to the dynamics of upwelling through the transition zone, or distortion may be caused by subduction-induced mantle flow. Topography of the 410 and 660 confirms that subducted slabs beneath the western U.S. are highly segmented, as inferred from recent tomography studies. We find no evidence of regionally pervasive velocity discontinuities between 750 and 1400 km depth. The plume's depth of origin within the lower mantle remains uncertain.

© 2012 Elsevier B.V. All rights reserved.

1. Introduction

Plume and non-plume origins have been suggested for Yellowstone hotspot volcanism because there are abundant observations that are consistent with the existence of a deep thermal upwelling (e.g., Smith et al., 2009) and also a similar abundance of observations that identify strong roles for lithospheric extension and subduction induced return flow in generation of widespread intra-plate volcanism since the mid-Miocene (e.g., Carlson and Hart, 1987). An important question is whether such upper mantle influences produce Yellowstone hotspot volcanism in the absence of an active lower mantle upwelling (Christiansen et al., 2002; Humphreys et al., 2000) or if they only serve to modulate melting processes that are triggered and spatially focused by a narrow active upwelling from the lower mantle. It is clear that Yellowstone hotspot activity occurs in the midst of tectonic conditions favorable to intra-plate volcanism, as volcanic rocks with Miocene and younger ages are distributed across much of western U.S. interior. Yet, Yellowstone hotspot volcanism stands out as exceptional within the western U.S. volcanism. Its concentration of magmatic productivity since 13 Ma, propagation of large caldera-forming rhyolitic eruptions parallel

to plate motion, correlation with a radially symmetric geoid high, and elevated ³He/⁴He Ra suggest that it may have a unique and deeper origin relative to the other western U.S. intra-plate volcanic activity (Fig. 1; Graham et al., 2009; Pierce and Morgan, 2009; Smith et al., 2009). New opportunities to investigate the mantle processes active beneath Yellowstone are afforded by the deployment of EarthScope's USArray (Fig. 1; www.earthscope.org).

Recent body-wave tomography using USArray data images low seismic velocities extending into the top of lower mantle beneath the Yellowstone hotspot (Burdick et al., 2009; James et al., 2011; Obrebski et al., 2010; Schmandt and Humphreys, 2010; Sigloch, 2011; Tian et al., 2011). However, there is no consensus as to whether this vertically irregular corridor of low-velocity mantle beneath Yellowstone should be interpreted as a local hot upwelling from the lower mantle. The proximity of high-velocity slabs motivates suggestions that upwelling beneath Yellowstone may be a purely upper mantle phenomenon driven by passive return flow in response to subduction (Faccenna et al., 2010; James et al., 2011). Unlike the thermal plume interpretation, these interpretations of Yellowstone's origin do not predict locally elevated temperature anomalies at the 410 or 660.

Seismically imaging mantle transition zone (MTZ) discontinuity topography provides a complementary means of evaluating whether a high-temperature anomaly is present across the lower–upper mantle

* Corresponding author.

E-mail address: schmandt@gps.caltech.edu (B. Schmandt).

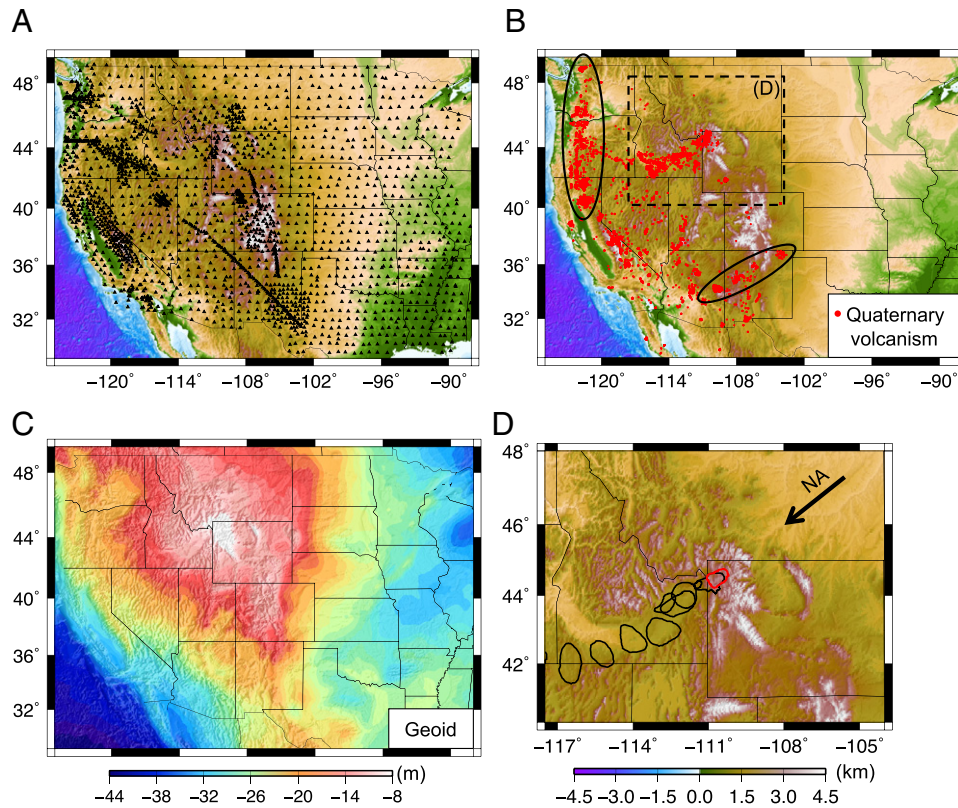


Fig. 1. Geography of the study area and geophysical and volcanic context for the Yellowstone hotspot. A) Map of the 2244 broadband seismic stations (black triangles) used for receiver function imaging. B) Locations of Quaternary volcanism (red dots) in the western U.S. from the NAVDAT database (Walker et al., 2004). The Cascades arc and Jemez lineament volcanic provinces discussed in the text (Section 4.2) are indicated (black ellipses). C) Geoid map (Smith and Milbert, 1999), which shows that the western U.S. lies within a broad geoid low and has a local maximum centered near the 0.6 Ma Yellowstone caldera. D) Locations of mapped rhyolitic calderas of the Yellowstone hotspot track (black contours) including the most recent, 0.6 Ma Yellowstone caldera (red contour). The direction of North America plate motion (black arrow) is indicated (Smith et al., 2009).

boundary beneath Yellowstone. Prior to deployment of USArray, receiver function imaging of the MTZ discontinuities in the Yellowstone region found depression of the 410 km discontinuity (410) near a low-velocity anomaly as expected for elevated temperatures. At this time, tomography did not find (and could not resolve) a low-velocity anomaly extending across the 660 km discontinuity (660), and receiver function imaging did not find an upward deflection of the 660, as would be expected for elevated temperatures (Fee and Dueker, 2004; Waite et al., 2006; Yuan and Dueker, 2005). Additionally, the location of the depressed 410 and correlative low-velocity anomaly in these studies is inconsistent with that of the low-velocity anomaly found in the MTZ by more recent tomography, which includes USArray and Yellowstone regional data (Schmandt and Humphreys, 2010). The more recent results have superior resolution at MTZ depths as a result of the wider aperture coverage including > 1300 new broadband stations.

In this study, we re-evaluate MTZ topography beneath the Yellowstone region, exploiting the complementary constraints of receiver functions from a dense wide-aperture array and the most complete 3-D P and S tomography models of the regional mantle. The primary new result is that the most upwarped patch of the 660 beneath USArray is centered about 75 km northeast of the 0.6 Ma Yellowstone caldera and coincides with the area where P and S tomography image low-velocities that extend from the MTZ down into the lower mantle. This suggests that Yellowstone hotspot volcanism is causally related to an active lower mantle upwelling.

2. Data and methods

The receiver function method (Langston, 1979; Vinnik, 1977) is used to isolate P-to-s (P_s) scattering from mantle discontinuities.

The raw data are three-component broadband seismogram segments of 450 s duration centered on teleseismic P arrivals from earthquakes with $M_b > 5.6$ and epicentral distances of 35–95°. These data were acquired from the IRIS DMC. In addition to data recorded by long-term networks and USArray, we use data from several dense PASSCAL arrays (Table 1 in Online Supplement) deployed over the past two decades for a total of 2244 stations. The three-component traces are rotated into P, S_v , S_h coordinates (Vinnik, 1977), and culled to isolate source-receiver pairs with good signal to noise ratio on both the P and S_v components. The signal to noise criterion requires the ratio of the root-mean-square (RMS) amplitudes to be > 3 for 4 s window compared to a 16 s window. Selected traces are aligned on the P-component arrival by multi-channel cross-correlation (VanDecar and Crosson, 1990).

A multi-channel spectral deconvolution method (Hansen and Dueker, 2009; Mercier et al., 2006) is used to separate the source waveform and the three-component (P, S_v , S_h) receiver functions. This deconvolution method is described in prior publications (Baig et al., 2005; Hansen and Dueker, 2009; Mercier et al., 2006) and briefly outlined here. A log-spectral least squares inversion is used to solve for the amplitude spectra of the sources and receiver functions (Mercier et al., 2006). With only the raw waveform data this inverse problem is under-determined so we augment (regularize) it with initial estimates of the source amplitude spectra. These initial estimates are calculated for each earthquake by fitting the observed P- S_v cross-spectra with smooth spline functions and stacking across regional sub-arrays. Sub-arrays with 6–8° aperture, rather than the entire operational USArray, are used for estimation of source spectra to avoid source radiation pattern modulation and other large distance variations. To exploit redundant sampling of similar source-receiver

geometries, the sources recorded by each station are binned by ray parameter (0.0035 s/km) and back-azimuth (10°) so that a single estimate of the three-component receiver function is obtained for each source bin. Because most stations operated for only 0.75–2 years the mean number of events per bin is 1.8, but source bins that sample high seismicity regions often include >5 events. The least-squares inversion only separates the amplitude spectra of the source and receiver functions. In order to recover their respective phase spectra, the P-component receiver function is assumed to be minimum phase (Bostock, 2004) and Kolmogorov spectral factorization is applied to construct a set of sequential all-pass filters that recover the phase spectra of the two transverse component (S_V , S_H) receiver functions (Mercier et al., 2006). In this paper, we present the S_V component receiver functions, which we bandpass filter between 50 s and 4 s.

A time versus ray-parameter (T-p) image made from 111,820 S_V component receiver functions illuminates Ps scattering from several near-horizontal velocity discontinuities, but also includes interference owing to later arriving PP and PcP phases (Fig. 2). A 1-D reference model was constructed that fits the arrival times of primary Ps phases as rendered in the T-p image. This reference model uses the mean of the TNA (Grand and Helmberger, 1984) and AK135 (Kennett et al., 1995) V_S models with a corresponding V_P model created using the V_P/V_S values of AK135. The timing of P410s and P660s phases depends on both the depth to the discontinuity and the path-integrated V_P and V_S above the discontinuity. Hence, accurate V_P and V_S models are required to isolate true discontinuity topography.

Receiver functions are mapped to position in the mantle using our 3-D V_P and V_S tomography models, which are slightly updated versions of those presented by Schmandt and Humphreys, 2010 and include USArray data up to June, 2011. The increase in data coverage adds some near-horizontal rays that sample the Yellowstone region at >700 km depth, but there are no dramatic changes in the Yellowstone low-velocity structure. The updated tomography inversions used the aforementioned TNA/AK135 hybrid reference model, but the change in reference model has little effect on the tomographically imaged structure because only teleseismic paths and relative travel-times are used. Receiver function Ps times are mapped to depth by extracting the V_P and V_S structure along the P and P_{DS} (D denotes discontinuity depth) ray paths in the tomography models and inserting the velocities in the 1-D spherical P_{DS} moveout equation. To avoid depth bias for the MTZ discontinuities a plane wave approximation is not used and instead we use a table of spherical P_{DS} ray-parameter values (Eagar et al., 2010; Lawrence and Shearer, 2006a). Because the tomography models account well for observed arrival time variations (variance reduction $>70\%$) our V_P and V_S travel-time corrections are considered to be very accurate.

Distributing the value of each S_V component receiver function over the width of its first Fresnel zone (dominant period of 5 s) is used to create a common conversion point (CCP) image volume (Dueker and Sheehan, 1997). The value of the CCP image in each 0.5° wide voxel is a weighted average with the receiver function weight normalized to be equal to unity within one half of the first Fresnel zone radius (R_{F1}) from the P_{DS} ray path and linearly decreasing to zero at R_{F1} . Typical R_{F1} dimensions are 95–135 km in the MTZ, depending on depth and epicentral distance. Similar weighted CCP approaches are commonly applied (Cao and Levander, 2010; Eagar et al., 2010; Lekic et al., 2011). The CCP stack uses only the portion of the receiver function prior to the PP arrival. Consequently, all the receiver functions contribute to the CCP stack at depths of <660 km but at 1400 km only 30% of them contribute.

To construct maps of the 410 and 660 interfaces from the CCP image, the depths of these two discontinuities are picked in each vertical column. The maximum value within a 70 km vertical window about the mean depth of each discontinuity (410 km, 656 km) is selected as the depth estimate. Bootstrap re-sampling of the image provides an estimate of discontinuity topography uncertainty in the

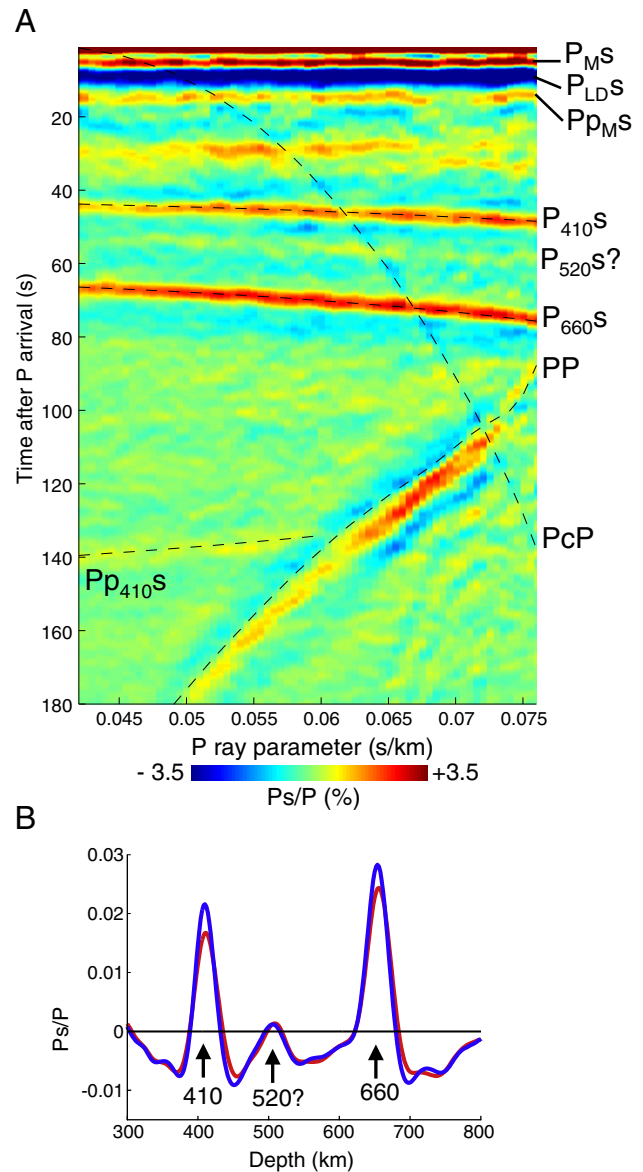


Fig. 2. Time versus ray-parameter (T-p) image and depth-migrated cumulative stack. A) Specific Ps and direct teleseismic phases are labeled, including Ps scattering from the Moho (M), lithospheric discontinuities (LD) (e.g., Fischer et al., 2010), 410, and 660. B) The cumulative depth-migrated stacks for 1-D (red) and 3-D (blue) velocity models are shown. Amplitudes of P_{410S} and P_{660S} increase by 24% and 14%, respectively. The increase in P_{410S} and P_{660S} amplitudes primarily results from the smaller standard deviations of 410 and 660 topography for receiver functions mapped to depth with the 3-D velocity models (Fig. 4).

depth picks (Efron and Tibshirani, 1986). Using 100 samples with 100% replacement the resulting 95% confidence intervals of 410 and 660 depth estimates are generally ≤ 6 km.

3. Results

The T-p image in Fig. 2A summarizes Ps conversions created by velocity discontinuities beneath USArray. The bright arrivals spanning the entire ray parameter range at 45–50 s and at 67–75 s exhibit the increase in arrival time with ray parameter expected for P410s and P660s. A cumulative stack of receiver functions mapped to depth shows these two prominent arrivals that bound the MTZ and also a local maxima near 520 km depth that may represent the 520 km discontinuity (Fig. 2B; Shearer, 1990). The 520 is routinely isolated by stacking SS and PP precursors

(e.g., Lawrence and Shearer, 2006b), but not imaged in global receiver function stacks (Chevrot et al., 1999; Lawrence and Shearer, 2006a; Tauzin et al., 2008). In addition to the P410s arrival we find a weaker Ps arrival that has decreasing arrival time with ray parameter as expected for the free-surface reflected and back-scattered Pp_{410s} phase (Fig. 2). Use of both forward-scattered and back-scattered phases from the MTZ will be the subject of future investigations, and at present detection of Pp_{410s} is noted to indicate that the quantity of data and deconvolution method employed can isolate this weak signal (~0.5–1% of P) associated with three transits through the upper 410 km. Arrivals displaying the moveout (relative to P) expected for Ps scattering from horizontal discontinuities at depths greater than 750 km are not observed.

Negative polarity arrivals adjacent to the P_{410s} and P_{660s} are observed, but are not coherent across the range of ray parameters (Fig. 2). Deconvolution and filtering induced side-lobes are estimated to have mean amplitude of 26% of their main pulse amplitude and should be coherent across the ray parameter range and hence side-lobes do not provide an adequate explanation for these arrivals. Side-lobe amplitude is estimated from the zero-lag arrival on the P-component receiver functions. Prior to the P_{410s} arrival and after P_{660s} the negative polarity segments of the depth-migrated stack show a more complex shape than a simple side-lobe indicating that interference from additional scattered arrivals is likely. Previous western North America studies using receiver functions and transition zone triplications identify velocity decreases with depth atop the MTZ (Eagar et al., 2010; Gilbert et al., 2003; Jasbinsek and Dueker, 2007; Schaeffer and Bostock, 2010; Schmandt et al., 2011; Song et al., 2004; Tauzin et al.,

2010; Vinnik et al., 2010) and, to a lesser extent, within the MTZ (Jasbinsek et al., 2010; Schmandt et al., 2011), but the depths of these discontinuities and their regional prevalence varies greatly. Scattering from discontinuities that are sporadically present or exhibit large lateral variations in depth will not stack coherently in our cumulative receiver function T–p image and must be investigated in a more regionalized manner, such as with CCP imaging.

Consistent with the T–p image the CCP images show nearly flat P410s and P660s horizons that are continuous across the image volume and a lack of laterally coherent arrivals beneath the MTZ (Fig. 3). Negative polarity arrivals adjacent to and within the MTZ are particularly prevalent beneath the Great Plains region and more sporadically present beneath the Cordillera. Some noteworthy deflections of the 410 and 660 are shown in Fig. 3B,D, which focuses on the region near the Yellowstone hotspot. Beneath Yellowstone the 660 is clearly deflected upward and the overlying 410 is approximately flat. The upward deflection of the 660 is centered northeast of the Yellowstone caldera by ~75 km. West of Yellowstone an upward deflection of the 410 is found beneath western Idaho, similar to earlier studies using USArray data (Fig. 3B; Cao and Levander, 2010; Eagar et al., 2010). In this study, we focus on our new results, which place Yellowstone mantle structure in a broad context including the U.S. Cordillera and a large portion of tectonically stable North America.

The depth distributions of 410 and 660 depths demonstrate the importance of lateral velocity variations in mapping MTZ discontinuity topography (Fig. 4). When correcting for P and S tomography structure the standard deviations of 410 and 660 depths are 6.8 km and 5.1 km,

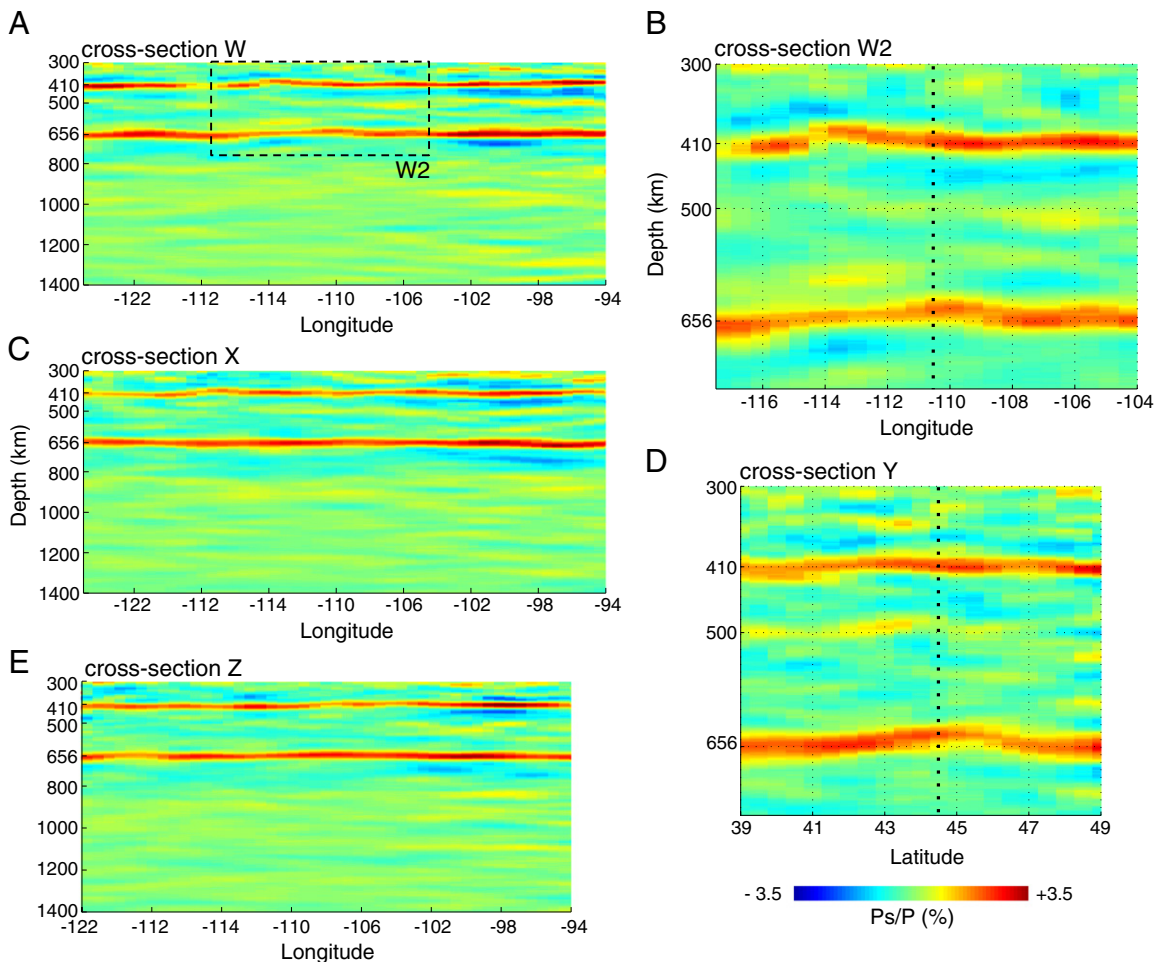


Fig. 3. Cross-sections through the CCP image. Locations of the cross-sections are indicated in Fig. 5A. Cross-sections in panels A, C, and E cover the entire west-to-east aperture of the study area. Cross-sections in B and D zoom in on the region of the Yellowstone hotspot. In panels B and D, the vertical dotted line denotes the horizontal position of the 0.6 Ma Yellowstone caldera.

respectively. If lateral velocity variations are ignored these values increase to 11.7 km (+72%) and 9.0 km (+76%), respectively. Maps of 410 and 660 topography created using only the 1-D velocity model show that the large lateral velocity contrast between the Cordillera and stable interior dominates the pattern of discontinuity topography (Fig. 5). In this case, both the 410 and 660 are anomalously deep in the southwest U.S. and shallow beneath the northeastern portion of the study region. The effect of lateral velocity variations on transition zone thickness is relatively subtle (Fig. 6) because MTZ thickness is less sensitive to the large lateral velocity variations in the uppermost mantle. Accurately mapping P410s and P660s to depth depends on the accuracy of the ray path integrated velocity structure above the discontinuities, but is little affected by the detailed velocity structure near the discontinuities. Given the excellent crossing-ray coverage and high variance reduction ($P = 78\%$, $S = 74\%$) of the tomography models we can be confident they provide greatly improved estimates of the path integrated velocity structure above the MTZ discontinuities.

The mean depths of the 410 and 660 are 410 km and 656 km, respectively, which are both within 3 km of a recent estimate of their global mean values determined by forward modeling global datasets of SS and PP precursors and Ps receiver functions (Lawrence and Shearer, 2006a, 2006b). The corresponding mean MTZ thickness of 246 km is slightly greater than the estimated global mean of 241–2 km (Lawrence and Shearer, 2006a, 2006b). We find greater peak-to-peak variations for the 410 (44 km) compared to the 660 (32 km), and large (>15 km) deflections are found beneath both Cordilleran and stable interior regions. Topography of the 410 (Fig. 5) shows that downward deflections of this discontinuity are much more

prevalent beneath the southwestern U.S. and west coast regions, whereas 660 topography does not exhibit a similar correlation.

The greatest upward deflection of the 660 found beneath the ~2000 km aperture study region is centered approximately 75 km northeast of the 0.6 Ma Yellowstone caldera (Fig. 5). A patch of the 660 that is 200–300 km wide is deflected upward by >12 km relative to the mean, with the central portion being deflected upward by up to 18 km (638 km). Gathering receiver functions that pierce this up-warped patch of the 660 demonstrates that the CCP stack that accounts for V_p and V_s tomography structure yields simple P660s pulses for receiver function stacks from separate groups of stations sampling the discontinuity from the northwest and southeast (Fig. 7A–D). The P660s maxima from these two groups are within 2 km. In contrast, gathers of receiver functions mapped to depth using only the 1-D reference model yield P660s pulses at different depths for the southeast and northwest station groups, including a bi-modal P660s pulse for the southeast stack (Fig. 7E,F). The dramatic increase in consistency of P660s pulses that sample the same region of the 660 but traverse different upper mantle velocity structures is a strong indication that improved estimates of discontinuity topography are obtained by using the V_p and V_s tomography models.

4. Discussion

4.1. Interpretation of 410 and 660 topography

Temperature, bulk and volatile composition, and convection may all give rise to topography of mantle phase transition and hence MTZ

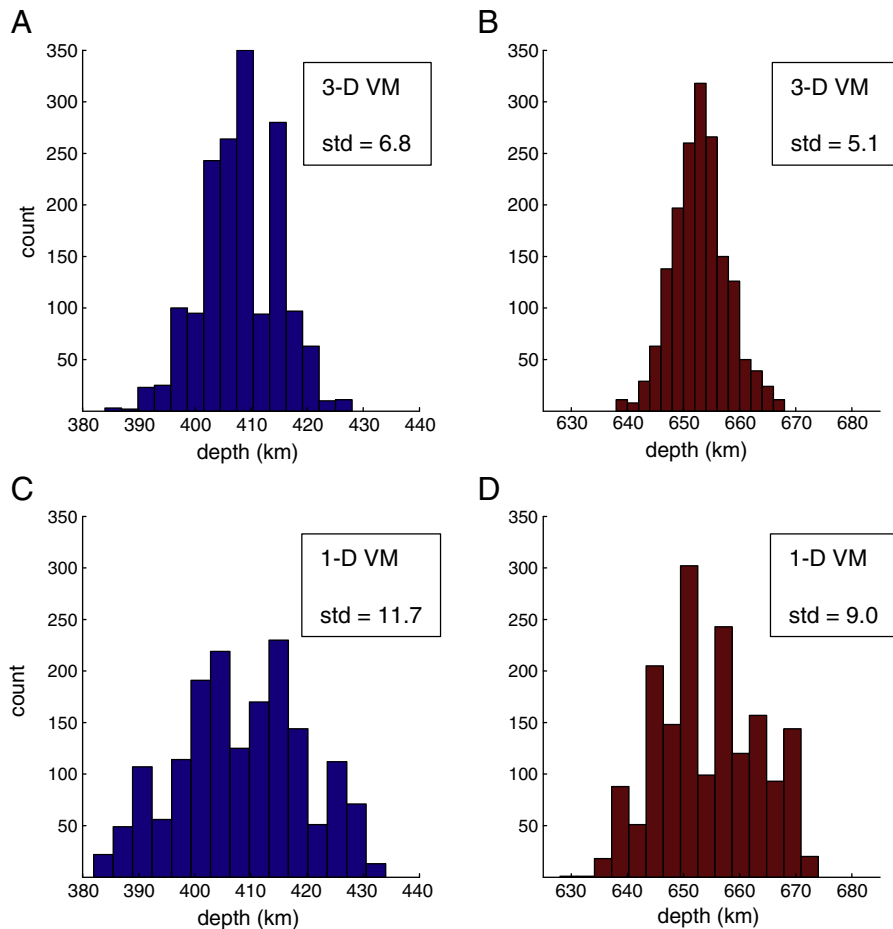


Fig. 4. Histograms of 410 and 660 topography. Histograms of topography derived by mapping the receiver functions through the 3-D tomography models are shown in A and B. Histograms of 410 and 660 topography derived using only the 1-D reference model (described in Section 2) are shown in C and D. The type of velocity model used and the standard deviation (std) are given in the upper right corner of each panel.

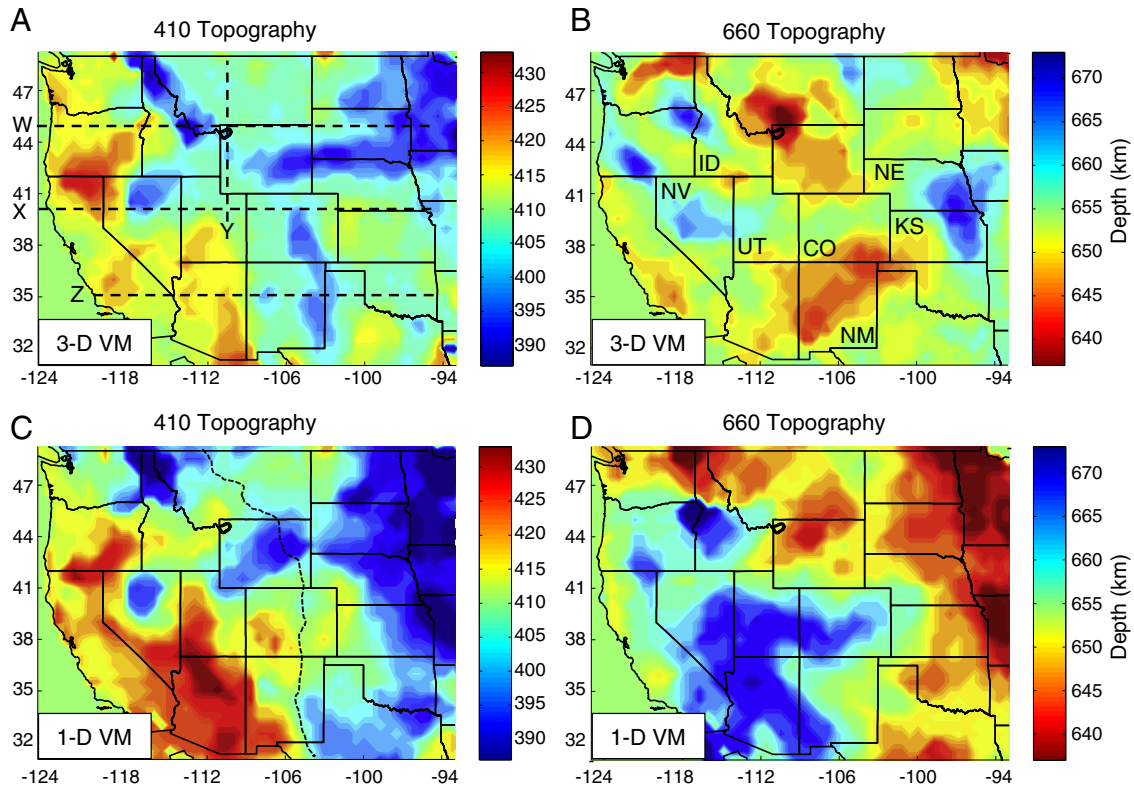


Fig. 5. Maps of 410 and 660 topography. Maps of topography, which account for lateral velocity variations imaged by 3-D V_p and V_s tomography are shown in A and B. Maps of topography, which ignore lateral velocity variations are shown in C and D. The type of velocity model used is given in the lower left corner of each panel. The straight dashed lines in A indicate the locations of the cross-sections shown in Fig. 3. The dashed contour in C denotes the Rocky Mountain front, which serves as the boundary between the tectonically and magmatically active Cordillera to west and the stable interior of North America to the east. Several U.S. states near prominent MTZ features are labeled: Nevada (NV), Idaho (ID), Utah (UT), Colorado (CO) New Mexico (NM), Kansas (KS), and Nebraska (NE).

discontinuities, but temperature variations are generally thought to be the most important influence on topography of the 410 and 660 and their effect currently is the best constrained (Helffrich, 2000). In the following discussion, features of 410 and 660 topography will be first considered in the context of thermal variations using Clapeyron slopes of 3.6 to 4 MPa/K for the olivine-to-wadsleyite transition at the 410 (Katsura et al., 2004; Morishima et al., 1994) and -1 to -2 MPa/K for the postspinel phase transition at the 660 (Fei et al., 2004; Katsura et al., 2003). Subsequently, the potential influences of non-thermal effects will be discussed acknowledging that these influences are not as well constrained.

4.2. Segmented slabs in the MTZ

Plate convergence in global plate tectonic reconstructions implies that >5000 km (trench-normal length) of ocean lithosphere has

subducted beneath the west coast of North America since 200 Ma (Engebretsen et al., 1985; Mueller et al., 2008), thus identifying a major source of thermal and chemical heterogeneity. Knowledge of the locations and continuity of subducted slabs beneath the western U.S. is important context for the origin of Yellowstone hotspot volcanism because if an active lower mantle upwelling exists it would have to interact with these structures. Cool temperatures of subducted slabs are expected to decrease the depth of the 410 and increase the depth of the 660, thus they should be manifest in our results.

Beneath the western portion of our study area, features of 410 and 660 topography consistent with cooler temperatures have been previously reported and primarily attributed to subducted slabs (Cao and Levander, 2010; Egar et al., 2010). Compared to prior studies, the upward deflections of the 410 that we image beneath northern Nevada and northern Idaho are similar in geometry but often have smaller magnitude (Fig. 5). Nearby depressions of the 660 were also

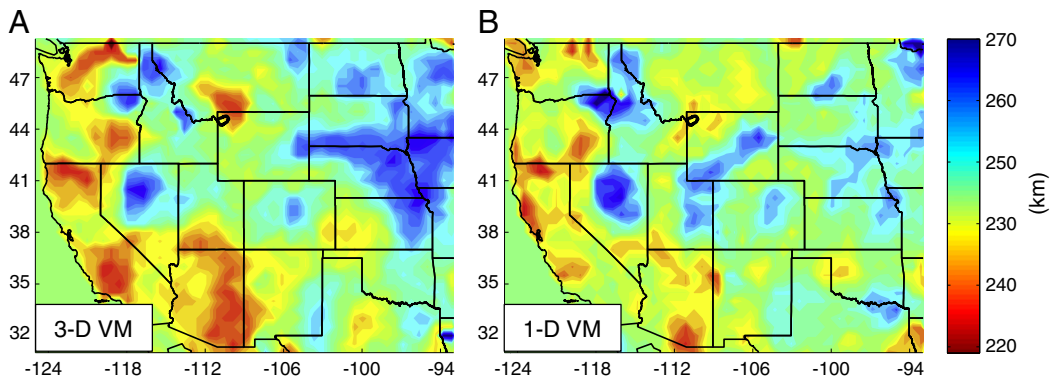


Fig. 6. MTZ thickness map. The MTZ thickness map obtained by accounting for 3-D V_p and V_s tomography is shown in A and the map obtained using only a 1-D velocity model is shown in B.

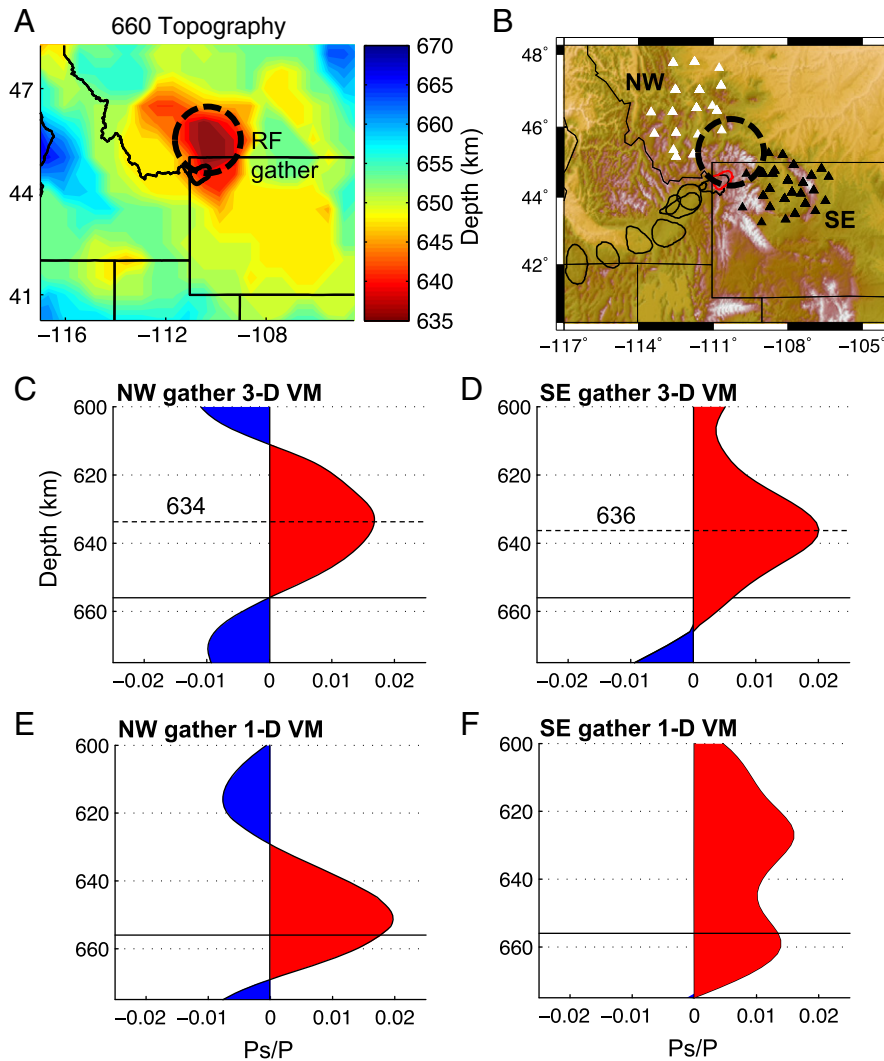


Fig. 7. Effects of 3-D velocity model on receiver function stacks sampling the 660 upwarp beneath the Yellowstone region. Receiver function stacks with P_{DS} rays that pierce 650 km depth within the black dashed circle in A and B and arrive at the northwest (NW) and southeast (SE) station groups shown in B are plotted and referred to as gathers in C–F. The gathers mapped to depth with the 3-D V_p and V_s tomography models are shown in C and D. Both of these have simple (rather than multi-modal) positive $P_{660\text{s}}$ pulses with maxima that are only 2 km apart (black dashed lines). Additionally both $P_{660\text{s}}$ maxima in C and D are clearly shallower than the mean 660 depth (black solid lines). The gathers mapped to depth with only the 1-D velocity model are shown in E and F, and these exhibit different $P_{660\text{s}}$ pulse shapes and maximal depths despite sampling the 660 in the same location. The SE gather in F has a bi-modal $P_{660\text{s}}$ pulse, which does not exist in the SE gather mapped to depth using the tomography models. These results indicate that the tomography models account well for lateral velocity variations because $P_{660\text{s}}$ pulses originating from the same portion of the 660 are expected to be consistent.

previously detected, though Cao and Levander (2010) found greater depression of the 660 beneath Utah. Agreement between the MTZ topography presented here and that of Cao and Levander (2010) is poorest near the eastern edge of their image, which is most simply explained by much less USArray data being available at the time their results were processed. In addition to these previously detected features, we find upward deflections of the 410 beneath the northern Great Plains and eastern Colorado and eastern New Mexico and depression of the 660 beneath Nebraska and Kansas (Fig. 5). Given the tectonic history of western North America we suggest subduction as the primary source for these volumes of cool mantle beneath the continental interior, though additional smaller contributions from cold downwellings of continental lithosphere are plausible.

A subduction origin for the newly detected deflections of the 410 and 660 beneath the Great Plains agrees well with Sigloch (2011), who inferred from tomography that some subducted segments remain in the upper mantle beneath the Great Plains while other, presumably older, slabs that lie farther west have already sunk beneath the 660. The updated tomography models herein significantly refine the geometry of the high-velocity features beneath the Great Plains

with >3 years of additional USArray data compared to Sigloch (2011) (Fig. 8). Generally, we do not favor a continental lithosphere origin for these features at 300–700 km depth because surface wave tomography and heat flow of the Great Plains imply that a thick (~200 km) lithosphere remains intact beneath most of the region (Pollack et al., 1993; Yuan et al., 2011). However, destabilization of continental lithosphere may explain the uplifted 410 beneath eastern New Mexico as tomographic imaging and waveform modeling suggest downwelling of depleted lithosphere near the southern end of the 410 upwarp (Gao et al., 2004; Song and Helmberger, 2007).

The magnitude of MTZ topography associated with these features includes upward deflections of the 410 by ~15–25 km and downward deflections of the 660 by ~8–15 km. Using the Clapeyron slopes mentioned in Section 4.1 we illustrate the implications of a purely thermal interpretation. Predicted thermal anomalies are 140–255 K and 160–590 K for the 410 and the 660, respectively. A standard geotherm for oceanic lithosphere and conductive warming in the mantle suggests 200–350 K thermal anomalies for slabs subducted since 50 Ma. More sophisticated models of <40 Ma western U.S. subduction predict similar thermal variations (Liu and Stegman, 2011).

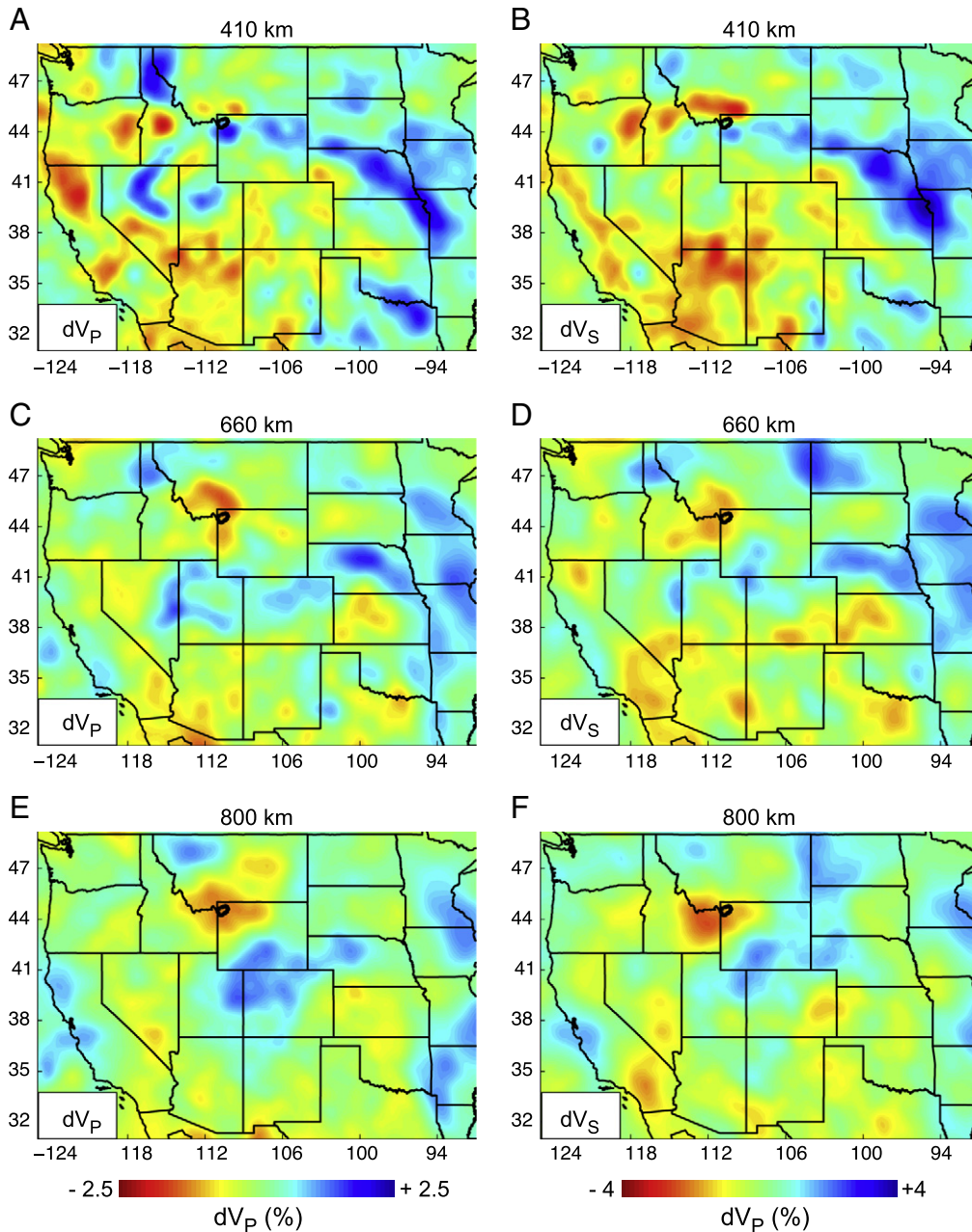


Fig. 8. Tomography maps. V_p and V_s tomography maps at 410 km (A,B), 660 km (C,D), and 800 km (E,F) are shown, with the color scale indicated at the bottom of each column. The tomography models are a slight update of those presented by Schmandt and Humphreys (2010) and they use the 1-D reference model described in Section 2.

The overlap in the ranges of temperature estimates for 410 and 660 is similar to the low end of expected temperature reductions for slabs (160–255 K), but large portions of the ranges are mutually exclusive. Relative to geodynamic expectations, purely thermal interpretations of 410 topography range from consistent to too small, whereas interpretations of 660 topography range from consistent to too large. Consequently, we suggest that factors other than temperature variations in pyrolite mantle are likely manifest in our detailed results, but to first order thermal interpretations are valid.

Can variations in volatile or bulk composition or the effects of vertical mantle flow lead to more satisfactory interpretations of MTZ topography associated with slabs? It is not clear whether slabs efficiently transport water into the MTZ (Green et al., 2010; Richard et al., 2006), and, if they do, high water content is expected to change 410 and 660 depths in the same direction as cooler temperatures (Frost and Dolejs, 2007; Litasov et al., 2005; Smyth and Frost, 2002).

Consequently, this effect cannot account for inconsistency in the magnitude of temperature variations inferred from the 410 and 660 unless slabs have greater water content at the 660 compared to the 410. We cannot rule out contributions to MTZ topography from water content in slabs (e.g., Cao and Levander, 2010), yet we note that invoking slab hydration in addition to temperature would not lead to better agreement between our results and thermal models of subduction (e.g., Liu and Stegman, 2011). In contrast, iron depletion of oceanic mantle lithosphere may offset thermal uplift of the 410 by as much as 7–10 km (Fei and Bertka, 1999), which could explain 410 uplift often being smaller than expected. Depending on local temperature and aluminum content, stabilization of additional phases near 660 km could affect imaged topography (Weidner and Wang, 1998), but we do not image multiple sharp velocity increases near 660 so the importance of this possibility is unclear. Vertical flow in the form of sinking slabs could modulate 410 and 660

topography provided that propagation of phase transformations is slower than flow rates (Solomatov and Stevenson, 1994). In general, downward flow of cool masses would damp topography of the 410 and amplify topography of the 660. Thus, kinetic effects could potentially explain underestimation of slab thermal perturbations at 410 and overestimation at 660, but if the regional MTZ is hydrated then phase transition kinetics will be too rapid to influence discontinuity topography (Diedrich et al., 2009; Kubo et al., 2004).

Our imaged MTZ topography supports the common inference from tomography that subducted slabs beneath the western U.S. are highly segmented (Burdick et al., 2009; James et al., 2011; Obrebski et al., 2010; Roth et al., 2008; Schmandt and Humphreys, 2010; Sigloch et al., 2008; Tian et al., 2011), as our discontinuity maps do not find continuous trench-parallel belts where the 410 is uplifted and the 660 is depressed. Additionally, if horizontal distance from the trench is taken as an indication of slab age then it appears that some slabs subducted about 50 Ma remain in the upper mantle beneath the Great Plains while some younger slabs have already sunk through the 660 beneath the Cordillera (e.g., Sigloch et al., 2008). The segmented state of slabs beneath the western U.S. and their apparently variable sinking rates make it difficult to infer the mantle flow field from tomography in a simple manner. This regional context is germane to understanding the origin of the Yellowstone hotspot because any potential active upwelling from the lower mantle must interact with this tectonically driven flow field and ascend through a gap between slab fragments prior to impinging upon the base of North America.

4.3. Hot mantle beneath Yellowstone

The origin of intra-plate volcanism, high heat flow, and high elevation in the western U.S. is a subject of considerable scrutiny and debate. Both active lower mantle upwellings (Suppe et al., 1975) and lateral displacement of North America over hot upper mantle of the East Pacific Rise (EPR) region (Cook, 1969; McKee, 1971) are longstanding suggestions. Geodynamic studies have also suggested that long-wavelength lower mantle upwelling may underlie the northern EPR itself (Forte et al., 2010). The new MTZ topography maps cover a large portion of the North America mantle, allowing the mantle structure beneath regions intra-plate volcanism to be viewed in a greater context than previously possible. This provides an opportunity to re-evaluate the relative importance of tectonic processes and active lower mantle upwellings for late Cenozoic western U.S. magmatic activity.

High temperature regions should exhibit depression of the 410 and upward deflection of the 660 (Fei et al., 2004; Katsura et al., 2003). Our mean MTZ thickness being ~4 km greater than global estimates (Section 3) suggests slightly cool mean MTZ temperature beneath the study area, but also isolated regions of high temperatures. The three most prominent examples are: upward 660 deflection of ≤ 18 km beneath the Yellowstone region, 410 depression of ≤ 14 km beneath the southern Cascades arc, and upward 660 deflection of ≤ 10 km beneath the Jemez volcanic lineament (Fig. 5). The Yellowstone and southern Cascades deflections are associated with a thin MTZ, whereas a broad elevated region of the 410 beneath New Mexico and Colorado results in MTZ thickness near the mean value beneath the Jemez lineament (Figs. 5, 6). In the southwestern U.S., smaller amplitude topography (~5 km) of the 410 and, to a lesser extent, the 660 is consistent with a broadly distributed warm region where the MTZ is generally 6–10 km thinner than the mean. Other Quaternary intra-plate volcanic fields are underlain by MTZ topography consistent with normal or relatively cool temperatures.

That the three most prominent features of MTZ topography consistent with high temperatures underlie Quaternary volcanic fields suggests causal relationships with heat sources in the MTZ or top of the lower mantle. Lack of vertical continuity between the 410 and

660 may result from mantle flow related to subduction and plate motion, or in cases where only 410 topography is anomalous upwelling may originate within the MTZ. For instance, the 410 depression beneath the southern Cascades could result from ascent of Pacific mantle stimulated by rollback of the Gorda slab, which extends continuously to only about 300 km depth where it is separated from deeper slabs (Chu et al., 2012; Schmandt and Humphreys, 2010). Tomographic images of low-velocity mantle adjacent to the Gorda slab support the presence of high temperatures near 400 km depth and such an anomaly is weak or absent near 660 km (Fig. 8; Schmandt and Humphreys, 2010; Xue and Allen, 2007). Additionally, compositional variations in southern Cascades volcanics have been attributed to upward flow of hot dry mantle (Elkins-Tanton et al., 2001). The location of the Jemez lineament correlates remarkably with a northeast trending 660 upwarp, but a correlative low-velocity anomaly is not imaged by tomography, making this feature difficult to interpret. The 660 upwarp beneath the Yellowstone region is the largest in amplitude and is accompanied by tomographically imaged low-velocities extending to about 900 km depth (Fig. 8; James et al., 2011; Obrebski et al., 2010; Schmandt and Humphreys, 2010; Sigloch, 2011; Tian et al., 2011). Together, these features strongly suggest active upwelling of hot lower mantle.

Among regions of intra-plate volcanism in the western U.S. the mantle structure beneath the Yellowstone hotspot track is unique and bears the strongest indications of active upwelling. In the shallow upper mantle (<150 km) seismic velocities beneath the eastern Snake River Plain (SRP) and Yellowstone caldera are the lowest in the western U.S. with V_S from surface wave (Lin et al., 2011) and body wave tomography ≤ 3.9 km/s. The ratio of V_S and V_P anomalies, often referred to as $R = \text{dln}V_S/\text{dln}V_P$, in body-wave tomography shows high R -values of 2.3–2.5 extending to 160–195 km depth beneath Yellowstone caldera and the easternmost SRP, which is consistent with melting at greater depth beneath this region than any other western U.S. volcanic field (Cammarano et al., 2003; Hammond and Humphreys, 2000; Schmandt and Humphreys, 2010). The very low V_S and depth extent of high R -values indicate anomalously hot upper mantle rather than passive upwelling alone. Upward deflection of the 660 and the corridor of low-velocities extending to ~900 km depth in USArray tomography models also are not explained by passive upwelling (e.g., Faccenna et al., 2010). This low-velocity anomaly is unlikely to be an artifact of a biased reference model because mean MTZ velocities beneath the western U.S. in global models range from slightly high (~1–2%) to globally nominal values (e.g., Lebedev and van der Hilst, 2008).

Using the Clapeyron slopes mentioned in Section 4.1, the 12–18 km deflection of the 660 corresponds to temperature increases of 235–700 K relative to the western U.S. mean. Body-wave tomography results predict temperature perturbations of 145–245 K at 600–700 km depth assuming $Q_S = 300$ (Dziewonski and Anderson, 1981) and the anelastic derivatives of Karato (1993). The difference between estimates suggests that factors in addition to temperature contribute to the 660 upwarp beneath the Yellowstone region or that the true postspinel Clapeyron slope in the western U.S. mantle is less than -1 MPa/K. These temperature estimates are expected to be higher than typical estimates of uppermost mantle plume excess temperatures (e.g., Putirka, 2008) for two reasons. First, cooling during plume ascent from 660 km to <100 km depth (where most melting occurs) will reduce the temperature contrast with ambient mantle by ~25% (Leng and Zhong, 2008). Second, the mean MTZ thickness beneath the western U.S. being ~4 km greater than the global mean suggesting that a small portion of the 660 upwarp may be attributed to cool surrounding mantle.

Non-thermal factors may be able to reconcile the unreasonably high maximum estimate of temperature beneath Yellowstone if the true post-spinel Clapeyron slope is near -1 MPa/K. A portion of the 660 upwarp beneath the Yellowstone region could be explained by

the ascent of relatively dry lower mantle into an MTZ that has been hydrated by subduction (Litasov et al., 2005). Water solubility in the nominally anhydrous minerals of the MTZ is greater than that in the lower mantle by about an order of magnitude (Inoue et al., 2010; Kohlstedt et al., 1996; Murakami et al., 2002), but uncertainty in the water content that is actually present precludes robust interpretation of this effect (Green et al., 2010; Karato, 2011; Yoshino et al., 2008). Kinetic effects owing to vertical mantle flow will be relatively small in high temperature upwellings compared to cold slabs, but may be possible (Solomatov and Stevenson, 1994). In general, subtle effects on 660 topography must be better constrained if the true postspinel Clapeyron slope is near -1 MPa/K because a contribution of only 3 km would change the temperature estimate by > 100 K.

Acknowledging the many uncertainties in estimating mantle temperature, we suggest that maximum temperatures near the 660 beneath Yellowstone are ~ 200 – 300 K higher than the western U.S. MTZ mean. Such temperatures could simultaneously satisfy V_p and V_s tomography and 660 topography, depending on the true postspinel Clapeyron slope and the importance of non-thermal effects. Higher temperature contrasts would likely imply absolute temperatures > 1800 K, at which the majorite-to-perovskite transformation is expected to be dominant and depression rather than shallowing of the discontinuity would be expected (Hirose, 2002). Based on the petrology of SRP basalts and tomography models that pre-date USArray, Leeman et al. (2009) infer a maximum excess temperature of 150 K at 70–100 km depth. Our temperature estimates at 660 corresponds to similar to somewhat greater excess temperatures of ~ 150 – 225 K at the same depth if we account for cooling during ascent from 660 (Leng and Zhong, 2008).

Within the lower mantle the depth of origin for the hot mantle extending across the 660 beneath Yellowstone remains uncertain. Plumes are expected to nucleate from thermal boundary layers, and the lack of global mid-mantle seismic discontinuities (Castle and van der Hilst, 2003; Vidale et al., 2001) and continuity of some subducted slabs in the lower mantle (Grand, 2002; Li et al., 2008) suggest that thermal boundary layers between the 660 and the D'' layer are unlikely. Our receiver functions also do not detect seismic discontinuities deeper than the 660 beneath the Yellowstone region. Thus, we favor a deep mantle origin and recognize that available USArray results can confidently track the thermal anomaly to about 900 km depth.

4.4. Pulsed upwelling

The absence of 410 deflection beneath the Yellowstone region and the vertical heterogeneity of the low-velocity anomaly (James et al., 2011; Obrebski et al., 2010; Schmandt and Humphreys, 2010; Sigloch, 2011; Tian et al., 2011) suggest significant differences from plumes generated in isolation of tectonically induced flow patterns and phase transitions (e.g., Lin and van Keken, 2006; Richards et al., 1989). The origin of the plume's irregular form cannot be uniquely determined from the seismic images, but we discuss effects that are likely to contribute to plume distortion. Radial viscosity variations (e.g., Hager and Richards, 1989) and mineral phase transitions (Hirose, 2002; Nishiyama and Yagi, 2003) are 1-D aspects of mantle structure that would tend to produce vertically heterogeneous plumes. Decreased viscosity and/or increased buoyancy contrast as the plume rises across the 660 are potential explanations for the change in geometry found in tomography (Fig. 9).

Interaction with a background flow-field likely affects the structure of all plumes (Steinberger, 2000), and slab-plume interaction is expected to be particularly important beneath Yellowstone (Geist and Richards, 1993; Obrebski et al., 2010; Schmandt and Humphreys, 2010; Tian et al., 2011). Hence, plume disruption by segmented sinking slabs and related return flow may cause the plume to be discontinuous as indicated by V_p tomography (Fig. 9). The V_s anomaly

exhibits greater continuity from 250 to 400 km depth, but its amplitude is diminished. Thus, strict continuity or discontinuity of the hot upwelling is not well constrained by the images, but the vertically heterogeneous geometry and magnitude of the V_p and V_s anomalies are quite similar (Fig. 9) and imply that a pulsating rather than uniform plume flux will reach the base of the lithosphere.

If the imaged seismic structure is characteristic of earlier mantle upwelling beneath the Yellowstone hotspot track, then manifestations of pulsing plume flux in the geologic record may be expected. It is noteworthy that the recurrence interval of caldera complex initiation along the Yellowstone hotspot track is ~ 3 m.y. and the recurrence interval of major caldera forming rhyolitic eruptions within each complex is ~ 0.7 m.y. (Pierce and Morgan, 2009). Aside from these discrete large-volume eruptions, overall productivity of the Yellowstone hotspot track has gradually declined since ~ 13 Ma (Pierce and Morgan, 2009). Magmatic flux variations with a range of different time-scales are observed at other hotspots such as Hawaii, which provides the most extensive and detailed record owing to its seamount chain dating back to ~ 80 Ma (van Ark and Lin, 2004; Vidal and Bonneville, 2004). Plume flux variations at the base of the lithosphere may contribute to such phenomena, in addition to evolving stress in the lithosphere (e.g., Hieronymus and Bercovici, 2001). Deeper origins of pulsating plume flux and hotspot magmatic productivity have also been proposed. Both numerical and analog experiments suggest that slight disturbances of deep plume conduits by large-scale flow can create solitary waves or diapir chains rather than vertically uniform conduits (Olson and Christensen, 1986; Schubert et al., 1989).

5. Conclusion

We have imaged topography of the 410 and 660 beneath the western U.S. with an unprecedented density and aperture of Ps receiver functions mapped to depth through V_p and V_s tomography models of the same area. Mean 410 and 660 depths are 410 km and 656 km. These depths imply that a mean MTZ thickness is ~ 4 km greater than the global mean suggesting slightly cooler mean temperature and/or enhanced water content, which are plausible considering the history of subduction. Beneath the Yellowstone hotspot region is the shallowest 660 of the entire study area with a maximal deflection of 18 km. The position of the 660 upwarp is consistent with a low V_p and V_s anomaly that extends from the top of the MTZ to about 900 km depth. Depth of the 410 beneath the Yellowstone region is near the mean depth. Between about 250 and 400 km the low V_p anomaly is disrupted and the low V_s anomaly is continuous but has diminished amplitude. Thus, MTZ topography and tomography images each indicate a vertically heterogeneous high temperature plume extending across the 660 beneath the Yellowstone hotspot. Because large volumes of anomalously hot mantle are thought to be generated only at thermal boundary layers and there is a lack of evidence for such boundaries between the 660 and D'' , we favor a lower mantle plume as the origin for the Yellowstone hotspot. It is clear that this plume must interact with segmented slabs present beneath the western U.S. in addition to radial viscosity variations and mineral phase transitions. We suggest these influences have disrupted the Yellowstone plume, specifically leading to absence of a large depression of the 410 and the vertically heterogeneous form of the low-velocity anomaly imaged by tomography.

Supplementary data to this article can be found online at doi:10.1016/j.epsl.2012.03.025.

Acknowledgments

Seismic data were acquired from the IRIS DMC. We thank the investigators responsible for the FACES, CAFE, SIEDCAR, HLP, Big Horns, and Ruby Mountains PASSCAL arrays for data access.

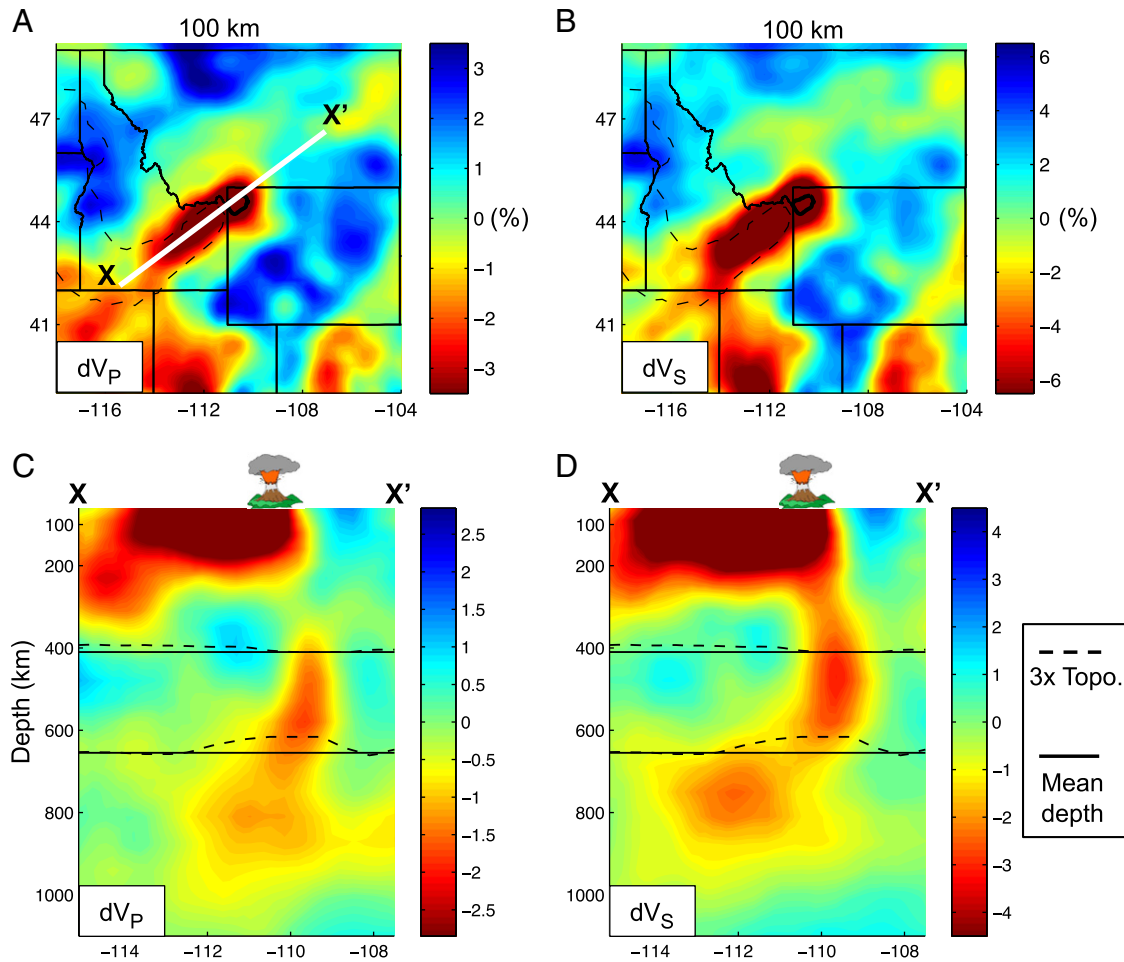


Fig. 9. Mantle cross-section through the eastern SRP and Yellowstone caldera. The location of the cross-section is shown on V_p and V_s tomography maps at 100 km in A and B, respectively. Cross-sections through the V_p and V_s models are shown in C and D, respectively. Exaggerated ($3\times$) 410 and 660 topography (black dashed) and mean depths (black line) are indicated. The color scale for the tomography images is shown on the right of each panel.

Discussions with Wei Leng, Fan-Chi Lin, and Victor Tsai are appreciated. We thank Nicholas Schmerr and Matt Fouch for constructive reviews, and Peter Shearer for editorial efforts. Seismic models can be obtained by contacting the corresponding author. This research was supported in part by the Gordon and Betty Moore Foundation. This is Caltech Tectonics Observatory Contribution #195. Additional support came from National Science Foundation grant EAR-0952194 to the University of Oregon.

References

- Baig, A.M., Bostock, M.G., Mercier, J.P., 2005. Spectral reconstruction of teleseismic P Green's functions. *J. Geophys. Res.* 110, B08306. doi:10.1029/2005JB003625.
- Bostock, M.G., 2004. Green's functions, source signatures, and the normalization of teleseismic wave fields. *J. Geophys. Res.* 109, B03303. doi:10.1029/2003JB002783.
- Burdick, S., et al., 2009. Model update December 2008: upper mantle heterogeneity beneath north America from travel time tomography with global and USArray transportable array data. *Seismol. Res. Lett.* 80 (4), 638–645.
- Cammarano, F., Goes, S., Vacher, P., Giardini, D., 2003. Inferring upper-mantle temperatures from seismic velocities. *Phys. Earth Planet. Inter.* 138, 197–222.
- Carlson, R.W., Hart, W.K., 1987. Crustal genesis on the Oregon Plateau. *J. Geophys. Res.* 92 (B7), 6191–6206. doi:10.1029/JB092iB07p06191.
- Cao, A., Levander, A., 2010. High-resolution transition zone structures of the Gorda Slab beneath the western United States: implication for deep water subduction. *J. Geophys. Res.* 115, B07301. doi:10.1029/2009JB006876.
- Castle, J.C., van der Hilst, R.D., 2003. Searching for seismic scattering off mantle interfaces between 800 km and 2000 km depth. *J. Geophys. Res.* 108 (B2), 2095.
- Chevrot, S., Vinnik, L.P., Montagner, J.-P., 1999. Global-scale analysis of the mantle Pds phases. *J. Geophys. Res.* 104, 20,203–20,219.
- Christiansen, R.L., Foulger, G.R., Evans, J.R., 2002. Upper-mantle origin of the Yellowstone hotspot. *Geol. Soc. Am. Bull.* 114, 1245–1256.
- Chu, R., Schmandt, B., Helmberger, D.V., 2012. Juan de Fuca subduction zone from a mixture of tomography and waveform modeling. *J. Geophys. Res.* 117, B03304. doi:10.1029/2012JB009146.
- Cook, K.L., 1969. Active rift system in the Basin and Range province. *Tectonophysics* 8, 469–511.
- Diedrich, T., Sharp, T.G., Leinenweber, K., Holloway, J.R., 2009. The effect of small amounts of H₂O on olivine to ringwoodite transformation growth rates and implications for subduction of metastable olivine. *Chem. Geol.* 262, 87–99.
- Dueker, K.G., Sheehan, A.F., 1997. Mantle discontinuity from mid-point stacks of converted P to S waves across the Yellowstone hotspot track. *J. Geophys. Res.* 102, 8313–8327. doi:10.1029/96JB03857.
- Dziewonski, A.M., Anderson, D.L., 1981. Preliminary reference Earth model. *Phys. Earth Planet. Inter.* 25, 297–356.
- Eagar, K.C., Fouch, M.J., James, D.E., 2010. Receiver function imaging of upper mantle complexity beneath the Pacific Northwest, United States. *Earth Planet. Sci. Lett.* 297, 141–153. doi:10.1016/j.epsl.2010.06.015.
- Efron, B., Tibshirani, R., 1986. Bootstrap methods for standard errors, confidence intervals, and other measures of statistical accuracy. *Stat. Sci.* 1, 54–75. doi:10.1214/ss/1177013815.
- Elkins-Tanton, L.T., Grove, T.L., Donnelly-Nolan, J., 2001. Hot shallow melting under the Cascades volcanic arc. *Geology* 29, 631–634.
- Engelbrechtsen, D.C., Cox, A., Gordon, R.G., 1985. Relative motions between oceanic and continental plates in the Pacific Basin. *Spec. Pap. Geol. Soc. Am.* 206, 560–569.
- Faccenna, C., Becker, T.W., Lallemand, S., Lagabrielle, Y., Funicello, F., Piromallo, C., 2010. Subduction triggered magmatic pulses: a new class of plumes? *Earth Planet. Sci. Lett.* 209, 54–68. doi:10.1016/j.epsl.2010.08.012.
- Fee, D., Dueker, K., 2004. Mantle transition zone topography and structure beneath the Yellowstone hotspot. *Geophys. Res. Lett.* 31, L18603. doi:10.1029/2004GL020636.
- Fei, Y., Bertka, C., 1999. Mantle Petrology: Field Observations and High Pressure Experimentation. In: Fei, Y., Bertka, C., Mysen, B. (Eds.), *Geochemical Society, Houston, TX*, vol. 6, pp. 189–207.
- Fei, Y., Van Orman, J., Li, J., van Westrenen, W., Sanloup, C., Minarik, W., Hirose, K., Komabayashi, T., Walter, M., Funakoshi, K., 2004. Experimentally determined postspinel transformation boundary in Mg₂SiO₄ using MgO as an internal pressure standard and its geophysical implications. *J. Geophys. Res.* 109, B02305. doi:10.1029/2003JB002562.

- Fischer, K.M., Ford, H.A., Abt, D.L., Rychert, C.A., 2010. The lithosphere–asthenosphere boundary. *Annu. Rev. Earth Planet. Sci.* 38, 551–575.
- Forté, A.M., Moucha, R., Simmons, N.A., Grand, S.P., Mitrovica, J.X., 2010. Deep mantle contributions to the surface dynamics of the North American continent. *Tectonophysics* 481 (1–4), 3–15.
- Frost, D.J., Dolejs, D., 2007. Experimental determination of the effect of H₂O on the 410 km seismic discontinuity. *Earth Planet. Sci. Lett.* 256 (1–2), 182–195. doi:10.1016/j.epsl.2007.01.023.
- Gao, W., Grand, S., Baldrige, W.S., Wilson, D., West, M., Ni, J., Aster, R., 2004. Upper mantle convection beneath the central Rio Grande rift imaged by P and S wave tomography. *J. Geophys. Res.* 109, B03305. doi:10.1029/2003JB002743.
- Geist, D., Richards, M., 1993. Origin of the Columbia Plateau and Snake River Plain: deflection of the Yellowstone plume. *Geology* 21, 789–792.
- Gilbert, H.J., Sheehan, A.F., Dueker, K.G., Molnar, P., 2003. Receiver functions in the western United States, with implications for upper mantle structure and dynamics. *J. Geophys. Res.* 108 (B5), 2229. doi:10.1029/2001JB001194.
- Graham, D.W., Reid, M.R., Jordan, B.T., Gruner, A.L., Leeman, W.P., Lupton, J.E., 2009. Mantle source provinces beneath the northwestern USA delimited by helium isotopes in young basalts. *J. Volcanol. Geotherm. Res.* 188, 128–140.
- Grand, S.P., Helmberger, D.V., 1984. Upper mantle shear structure of North America. *Geophys. J. R. Astron. Soc.* 76, 399–438.
- Grand, S.P., 2002. Mantle shear wave tomography and the fate of subducted slabs. *Philos. Trans. R. Soc. Lond. A* 360, 2475–2491.
- Green, H.W., Chen, W.-P., Brudzinski, M.R., 2010. Seismic evidence of negligible water carried below 400 km depth in subducting lithosphere. *Nature* 467 (7317), 828–831. doi:10.1038/nature09401.
- Hager, B.H., Richards, M.A., 1989. Long-wavelength variations in Earth's geoid – physical models and dynamic implications. *Philos. Trans. R. Soc. A* 328, 309–327.
- Hammond, W.C., Humphreys, E.D., 2000. Upper mantle seismic wave velocity: effects of realistic partial melt geometries. *J. Geophys. Res.* 105 (B5), 975–986.
- Hansen, S., Dueker, K., 2009. P and S wave receiver function images of crustal imbrication beneath the Cheyenne belt in southeast Wyoming. *Bull. Seismol. Soc. Am.* 99, 1953–1961. doi:10.1785/0120080168.
- Helffrich, G., 2000. Topography of the transition zone seismic discontinuities. *Rev. Geophys.* 38, 141–158. doi:10.1029/1999RG000060.
- Hieronymus, C.F., Bercovici, D., 2001. A theoretical model of hotspot volcanism: control on volcanic spacing and patterns via magma dynamics and lithospheric stresses. *J. Geophys. Res.* 106, 683–702. doi:10.1029/2000JB900355.
- Hirose, K., 2002. Phase transitions in pyrolytic mantle around 670 km depth: implications for upwelling of plumes from the lower mantle. *J. Geophys. Res.* 107, 2078.
- Humphreys, E.D., Dueker, K.G., Schutt, D.L., Smith, R.B., 2000. Beneath Yellowstone: evaluating plume and nonplume models using teleseismic images of the upper mantle. *GSA Today* 10 (12), 1–7.
- Inoue, T., Wada, T., Sasaki, R., Yurimoto, H., 2010. Water partitioning in the Earth's mantle. *Phys. Earth Planet. Inter.* 183, 245–251.
- James, D.E., Fouch, M.J., Carlson, R.W., Roth, J.B., 2011. Slab fragmentation, edge flow and the origin of the Yellowstone hotspot track. *Earth Planet. Sci. Lett.* doi:10.1016/j.epsl.2011.09.007.
- Jasbinsk, J., Dueker, K.G., 2007. Ubiquitous low-velocity layer atop the 410 km discontinuity in the northern Rocky Mountains. *Geochem. Geophys. Geosyst.* 8, Q10004. doi:10.1029/2007GC001661.
- Jasbinsk, J.J., Dueker, K.G., Hansen, S.M., 2010. Characterizing the 410 km discontinuity low-velocity layer beneath the LA RISTRA array in the North American Southwest. *Geochem. Geophys. Geosyst.* 11, Q03008. doi:10.1029/2009GC002836.
- Karato, S., 1993. Importance of anelasticity in the interpretation of seismic tomography. *Geophys. Res. Lett.* 20, 1623–1626.
- Karato, S., 2011. Water distribution across the mantle transition zone and its implications for the global material cycle. *Earth Planet. Sci. Lett.* 301, 413–423. doi:10.1016/j.epsl.2010.11.038.
- Katsura, T., et al., 2003. Post-spinel transition in Mg₂SiO₄ determined by in situ X-ray diffractometry. *Phys. Earth Planet. Inter.* 136, 11–24.
- Katsura, T., et al., 2004. Olivine–wadsleyite transition in the system (Mg, Fe)₂SiO₄. *J. Geophys. Res.* 109, B02209. doi:10.1029/2003JB002438.
- Kennett, B.L.N., Engdahl, E.R., Buland, R.P., 1995. Constraints on seismic velocities in the Earth from travel times. *Geophys. J. Int.* 122, 108–124. doi:10.1111/j.1365-246X.1995.tb03540.x.
- Kohlstedt, D., Keppler, H., Rubie, D., 1996. Solubility of water in the alpha, beta and gamma phases of (Mg, Fe)(2)SiO₄. *Contrib. Mineral. Petrol.* 123 (4), 345–357.
- Kubo, T., Ohtani, E., Funakoshi, K., 2004. Nucleation and growth kinetics of the alpha-beta transformation in Mg₂SiO₄ determined by in-situ synchrotron X-ray powder diffraction. *Am. Mineral.* 89, 285–293.
- Langston, C., 1979. Structure under Mount Rainier, Washington, inferred from teleseismic body waves. *J. Geophys. Res.* 84 (B9), 4749–4762.
- Lawrence, J.F., Shearer, P.M., 2006a. Constraining seismic velocity and density for the mantle transition zone with reflected and transmitted waveforms. *Geochem. Geophys. Geosyst.* 7, Q10012. doi:10.1029/2006GC001339.
- Lawrence, J.F., Shearer, P.M., 2006b. A global study of transition zone thickness using receiver functions. *J. Geophys. Res.* 111, B06307. doi:10.1029/2005JB003973.
- Lebedev, S., van der Hilst, R., 2008. Global upper mantle tomography with the automated inversion of surface and S-waveforms. *Geophys. J. Int.* 173, 505–518. doi:10.1111/j.1365-246X.2008.03721.x.
- Leeman, Schutt, D.L., Hughes, S.S., 2009. Thermal structure beneath the Snake River Plain: implications for the Yellowstone hot spot. *J. Volcanol. Geotherm. Res.* 188, 57–67.
- Leng, W., Zhong, S., 2008. Controls on plume heat flux and plume excess temperature. *J. Geophys. Res.* 113, B04408. doi:10.1029/2007JB005155.
- Lekic, V., French, S.W., Fischer, K.M., 2011. Lithospheric thinning beneath rifted regions of southern California. *Science* 334 (6057), 783–787. doi:10.1126/science.1208898.
- Li, C., van der Hilst, R.D., Engdahl, E.R., Burdick, S., 2008. A new global model for P wave speed variations in Earth's mantle. *Geochem. Geophys. Geosyst.* 9, Q05018. doi:10.1029/2007GC001806.
- Lin, F.C., Ritzwoller, M.H., Yang, Y., Moschetti, M., Fouch, M., 2011. Complex and variable crustal and uppermost mantle seismic anisotropy in the western United States. *Nat. Geosci.* 4, 55–61. doi:10.1038/ngeo1036.
- Lin, S.-C., van Keken, P.E., 2006. Deformation, stirring and material transport in thermochemical plumes. *Geophys. Res. Lett.* 33, L20306. doi:10.1029/2006GL027037.
- Litasov, K., Ohtani, E., Sano, A., Suzuki, A., 2005. Wet subduction versus cold subduction. *Geophys. Res. Lett.* 32, L13312. doi:10.1029/2005GL022921.
- Liu, L., Stegman, D.R., 2011. Segmentation of the Farallon slab. *Earth Planet. Sci. Lett.* 311, 1–10.
- McKee, E.H., 1971. Tertiary igneous chronology of the Great Basin of western United States – implications for tectonic models. *Geol. Soc. Am. Bull.* 82, 3497–3502.
- Mercier, J.P., Bostock, M.G., Baig, A.M., 2006. Improved Green's functions for passive source structural studies. *Geophysics* 71 (4), S195–S1102. doi:10.1190/1.2213951.
- Morishima, H., Kato, T., Suto, M., Ohtani, E., Urakawa, S., Utsumi, W., Shimomura, O., Kikegawa, T., 1994. The phase boundary between alpha and beta Mg₂SiO₄ determined by in situ X-ray observation. *Science* 265, 1202–1203.
- Mueller, R.D., Sdrolias, M., Gaina, C., Roest, W.R., 2008. Age, spreading rates and spreading asymmetry of the world's ocean crust. *Geochem. Geophys. Geosyst.* 9, Q04006. doi:10.1029/2007GC001743.
- Murakami, M., Hirose, K., Yurimoto, H., Nakashima, S., Takafuji, N., 2002. Water in Earth's lower mantle. *Science* 295, 1885–1887.
- Nishiyama, N., Yagi, T., 2003. Phase relation and mineral chemistry in pyrolite to 2200 °C under the lower mantle pressures and implications for dynamics of mantle plumes. *J. Geophys. Res.* 108 (B5), 2255.
- Obrebski, M., Allen, R.M., Xue, M., Hung, S., 2010. Slab–plume interaction beneath the Pacific Northwest. *Geophys. Res. Lett.* 37, L14305. doi:10.1029/2010GL043489.
- Olson, P., Christensen, U., 1986. Solitary wave propagation in a fluid conduit within a viscous matrix. *J. Geophys. Res.* 91, 6367–6374.
- Pierce, K.L., Morgan, L.A., 2009. Is the track of the Yellowstone hotspot driven by a deep mantle plume? – a review of volcanism, faulting, and uplift in light of new data. *J. Volcanol. Geotherm. Res.* 188, 1–25.
- Pollack, H.N., Hurter, S.J., Johnson, J.R., 1993. Heat flow from the Earth's interior: analysis of the global data set. *Rev. Geophys.* 31, 267–280.
- Putirka, K.D., 2008. Excess temperatures at ocean islands: implications for mantle layering and convection. *Geology* 36, 283–286.
- Richard, G., Bercovici, D., Karato, S., 2006. Slab dehydration in the Earth's mantle transition zone. *Earth Planet. Sci. Lett.* 251, 156–167. doi:10.1016/j.epsl.2006.09.006.
- Richards, M., Duncan, R., Courtillot, V., 1989. Flood basalts and hotspot tracks: plume heads and tails. *Science* 246 (4926), 103–107.
- Roth, J.B., Fouch, M.J., James, D.E., Carlson, R.W., 2008. Three-dimensional seismic velocity structure of the northwestern United States. *Geophys. Res. Lett.* 35, L15304. doi:10.1029/2008GL034669.
- Schaeffer, A.J., Bostock, M.G., 2010. A low-velocity zone atop the transition zone in northwestern Canada. *J. Geophys. Res.* 115, B06302. doi:10.1029/2009JB006856.
- Shearer, P.M., 1990. Seismic imaging of upper mantle structure with new evidence for a 520 km discontinuity. *Nature* 344, 121–126. doi:10.1038/344121a0.
- Schmandt, B., Humphreys, E., 2010. Complex subduction and small-scale convection revealed by body-wave tomography of the western United States upper mantle. *Earth Planet. Sci. Lett.* 297, 435–445. doi:10.1016/j.epsl.2010.06.047.
- Schmandt, B., Dueker, K.G., Hansen, S.M., Jasbinsk, J.J., Zhang, Z., 2011. A sporadic low-velocity layer atop the western U.S. mantle transition zone and short-wavelength variations in transition zone discontinuities. *Geochem. Geophys. Geosyst.* 12, Q08014. doi:10.1029/2011GC003668.
- Schubert, G., Olson, P., Anderson, C., Goldman, P., 1989. Solitary waves in mantle plumes. *J. Geophys. Res.* 94, 9523–9532.
- Sigloch, K., McQuarrie, N., Nolet, G., 2008. Two-stage subduction history under North America inferred from multiple-frequency tomography. *Nat. Geosci.* 1, 458–462.
- Sigloch, K., 2011. Mantle provinces under North America from multi-frequency P wave tomography. *Geochem. Geophys. Geosyst.* 12, Q02W08. doi:10.1029/2010GC003421.
- Smith, D.A., Milbert, D.G., 1999. The GEIOD96 high resolution geoid height model for the United States. *J. Geod.* 73 (5), 219–236.
- Smith, R.B., et al., 2009. Geodynamics of the Yellowstone hotspot and mantle plume: seismic and GPS imaging, kinematics, and mantle flow. *J. Volcanol. Geotherm. Res.* 188, 26–56.
- Smyth, J.R., Frost, D.J., 2002. The effect of water on the 410 km discontinuity: an experimental study. *Geophys. Res. Lett.* 29 (10), 1485. doi:10.1029/2001GL014418.
- Solomatov, V.S., Stevenson, D.J., 1994. Can sharp seismic discontinuities be caused by non-equilibrium phase transformations? *Earth Planet. Sci. Lett.* 125, 267–279.
- Song, T.A., Helmberger, D.V., 2007. P and S waveform modeling of continental sub-lithospheric detachment at the eastern edge of the Rio Grande Rift. *J. Geophys. Res.* 112, B07319. doi:10.1029/2007JB004942.
- Song, T.A., Helmberger, D.V., Grand, S.P., 2004. Low velocity zone atop the 410 seismic discontinuity in the northwestern United States. *Nature* 427, 530–533. doi:10.1038/nature02231.
- Steinberger, B., 2000. Plumes in a convecting mantle: models and observations from individual hotspots. *J. Geophys. Res.* 105, 11,127–11,152.
- Suppe, J., Powell, C., Berry, R., 1975. Regional topography, seismicity, Quaternary volcanism, and the present-day tectonics of the western United States. *Am. J. Sci.* 275 (A), 397–436.

- Tauzin, B., Debayle, E., Wittlinger, G., 2008. The mantle transition zone as seen by global Pds phases: no clear evidence for a thin transition zone beneath hotspots. *J. Geophys. Res.* 113, B08309. doi:10.1029/2007JB005364.
- Tauzin, B., Debayle, E., Wittlinger, G., 2010. Seismic evidence for a global low velocity layer in the Earth's upper mantle. *Nat. Geosci.* 3, 718–721. doi:10.1038/ngeo969.
- Tian, Y., Zhou, Y., Sigloch, K., Nolet, G., Laske, G., 2011. Structure of North American mantle constrained by simultaneous inversion of multiple-frequency SH, SS, and Love waves. *J. Geophys. Res.* 116, B02307. doi:10.1029/2010JB007704.
- van Ark, Lin, E.J., 2004. Time variation in igneous volume flux of the Hawaii–Emperor hot spot seamount chain. *J. Geophys. Res.* 109, B11401.
- VanDecar, J.C., Crosson, R., 1990. Determination of teleseismic relative phase arrival times using multi-channel cross-correlation and least squares. *Bull. Seismol. Soc. Am.* 80, 150–159.
- Vidal, V., Bonneville, A., 2004. Variations of the Hawaiian hot spot activity revealed by variations in the magma production rate. *J. Geophys. Res.* 109, B03104. doi:10.1029/2003JB002559.
- Vidale, J.E., Schubert, G., Earle, P.S., 2001. Unsuccessful initial search for a mid mantle chemical boundary with seismic arrays. *Geophys. Res. Lett.* 28, 859–862.
- Vinnik, L., 1977. Detection of waves converted from P to SV in the mantle. *Phys. Earth Planet. Inter.* 67, 39–45.
- Vinnik, L., Ren, Y., Stutzmann, E., Farra, V., Kiselev, S., 2010. Observations of S410p and S350p phases at seismograph stations in California. *J. Geophys. Res.* 115, B05303. doi:10.1029/2009JB006582.
- Waite, G.P., Smith, R.B., Allen, R.M., 2006. Vp and Vs structure of the Yellowstone hot spot: evidence for an upper mantle plume. *J. Geophys. Res.* 111 (B4), B04303. doi:10.1029/2005JB003867.
- Walker, J.D., Bowers, T.D., Glazner, A.F., Farmer, A.L., Carlson, R.W., 2004. Creation of a North American volcanic and plutonic rock database (NAVDAT). *Geological Society of America Abstracts with Programs*, vol. 36, no. 4, p. 9.
- Weidner, D., Wang, Y., 1998. Chemical and Clapeyron induced buoyancy at the 660 km discontinuity. *J. Geophys. Res.* 103, 7431–7441. doi:10.1029/97JB03511.
- Xue, M., Allen, R.M., 2007. The fate of the Juan de Fuca plate: implications for a Yellowstone plume head. *Earth Planet. Sci. Lett.* 264, 266–276. doi:10.1016/j.epsl.2007.09.047.
- Yoshino, T., Manthilake, G., Matsuzaki, T., Katsura, T., 2008. Dry mantle transition zone inferred from the conductivity of wadsleyite and ringwoodite. *Nature* 451, 326–329. doi:10.1038/nature06427.
- Yuan, H., Dueker, K., 2005. Teleseismic P-wave tomogram of the Yellowstone plume. *Geophys. Res. Lett.* 32, L07304. doi:10.1029/2004FL022056.
- Yuan, H., Romanowicz, B., Fischer, K.M., Abt, D., 2011. 3-D shear wave radially and azimuthally anisotropic velocity model of the North American upper mantle. *Geophys. J. Int.* 184, 1237–1260. doi:10.1111/j.1365-246X.2010.04901.x.